MAGNET SYSTEMS
FOR LARGE PARTICLE ACCELERATORS

Arnaud Devred
(arnaud.devred@cea.fr)

Commissariat à l'Energie Atomique de Saclay (CEA/Saclay)
DSM/DAPNIA/STCM
F–91191 GIF-SUR-YVETTE CEDEX
FRANCE

and

CERN, Laboratoire Européen pour la Physique des Particles
LHC/MMS
CH–1211 GENEVE 23
SUISSE

ABSTRACT

After a brief description of the various types of high-energy particle accelerators (sections 1 and 2), we review the principles of charged particle acceleration, guiding and focusing, and we introduce the basic formulae to compute synchrotron radiation (section 3). Next, we detail the layout of large circular machines, and we illustrate it by the Large Hadron Collider (LHC), now under development at the European Laboratory for Particle Physics (CERN), (section 4). Finally, we explain the field parameters and the functions of dipole and quadrupole magnets (section 5), and we compare the configurations of detector magnets (section 6).

FOREWORD

This paper is a work in progress and is part of a broader review that was prepared initially for the Wiley Encyclopedia of Electrical and Electronics Engineering. Previous versions of it can be found in

• A. Devred, "Superconducting magnets for particle accelerators and storage rings." In J.G. Webster (ed.), *Wiley Encyclopedia of Electrical and Electronics Engineering*, New York, NY: John Wiley & Sons, Vol. 20, pp. 743–762, 1999.

• A. Devred, "Review of superconducting storage-ring dipole and quadrupole magnets." In S. Turner (ed.), *Proc. of CERN Accelerator School on Measurement and Alignment of Accelerator and Detector Magnets*, CERN 98–05, Geneva, Switzerland: CERN, pp. 43–78, 1998.

• A. Devred, "Review of superconducting dipole and quadrupole magnets for particle accelerators," DAPNIA/STCM Preprint 98–07, Gif-sur-Yvette, France: CEA/Saclay DSM/DAPNIA, August 1998.

• A. Devred, "1999 Review of superconducting dipole and quadrupole magnets for particle accelerators," DAPNIA/STCM Preprint 99–24, Gif-sur-Yvette, France: CEA/Saclay DSM/DAPNIA, December 1999.

Compared to the last version, the main additions are: some historical background on particle accelerators (section 1), an introduction to synchrotron radiation (section 3.5), and a comparison of detector magnet configurations (section 6).

Comments and suggestions are welcome.

CONTENTS

ACRONYMS

ALEPH	**A**pparatus for **LE**P **PH**ysics
ATLAS	**A**ir core **T**oroid for **L**arge **A**cceptance **S**pectrometer or **A** **T**oroidal **L**HC **A**pparatu**S**
BT	**B**arrel **T**oroid
CMS	**C**ompact **M**uon **S**olenoid
CEA	**C**ommissariat à l'**E**nergie **A**tomique (Atomic Energy Commission)
CERN	European Laboratory for Particle Physics (formerly, **C**entre **E**uropéen pour la **R**echerche **N**ucléaire)
CS	**C**entral **S**olenoid
DELPHI	**DE**tector with **L**epton, **P**hoton and **H**adron **I**dentification
DESY	**D**eutsches **E**lektronen-**SY**nchrotron (German Electron Synchrotron)
ECT	**E**nd **C**ap **T**oroid
ETH	**E**igenössiche **T**ecknische **H**ochschule (Swiss Federal Institute of Technology)
INFN	**I**stituto **N**ationali di **F**isica **N**ucleare (National Institute for Nuclear Physics)
KEK	High Energy Accelerator Research Organization
LEP	**L**arge **E**lectron **P**ositron collider
LINAC	**LIN**ear **AC**celerator
LHC	**L**arge **H**adron **C**ollider
OPAL	**O**mni **P**urpose **A**pparatus at **L**EP
PS	**P**roton **S**ynchrotron
R&D	**R**esearch **and D**evelopment
RAL	**R**utherford **A**ppleton **L**aboratory
RF	**R**adio **F**requency
PSB	**P**roton **S**ynchrotron **B**ooster
SLAC	**S**tandford **L**inear **A**ccelerator **C**enter
SLC	**S**tanford **L**inear **C**ollider
SPS	**S**uper **P**roton **S**ynchrotron
TESLA	**T**era **E**lectron volts **S**uperconducting **L**inear **A**ccelerator
USA	**U**nited **S**tates of **A**merica

NOMENCLATURE

ROMAN LETTERS

a_q	Component of the acceleration of a particle of charge, q, perpendicular to its direction of motion (m^2/s).
B	Modulus of $\vec{B}$ (T).
$\vec{B}$	Magnetic flux density vector.
B_0	Axial or circumferential field strength (T).
B_1	Dipole field strength or normal dipole field coefficient (T).
B_r	Radial component of $\vec{B}$ in a cylindrical coordinate system.
B_θ	Azimuthal component of $\vec{B}$ in a cylindrical coordinate system.
B_x, B_y, B_z	x-, y- and z-components of $\vec{B}$ in a rectangular coordinate system.
c = 299 792 458 m/s	Speed of light in free space.
cot( )	Cotangent function.
coth( )	Hyperbolic cotangent function.
$\vec{E}$	Electric field vector.
$\overrightarrow{F_C} = q\,\vec{E}$	Coulomb's force vector.
$\overrightarrow{F_L} = q\,\overrightarrow{v_q} \times \vec{B}$	Lorentz' force vector.
$f_{quad} \approx \frac{1}{\sqrt{\kappa_g}} \cot\left(\sqrt{\kappa_g}\, l_{quad}\right)$	Normal quadrupole magnet focusing length (m).
$f'_{quad} \approx \frac{-1}{\sqrt{\kappa_g}} \coth\left(\sqrt{\kappa_g}\, l_{quad}\right)$	Normal quadrupole magnet defocusing length (m).
g	Quadrupole field gradient (T/m).
l_{dip}	Magnetic length of a dipole magnet (m).
l_{quad}	Magnetic length of a quadrupole magnet (m).
m_e	Mass at rest of a charged particle in units of electron mass at rest (dimensionless).
m_q	Mass at rest of a particle of charge, q (kg).
O	A given point of the design orbit of an accelerator ring.
P_q	Power radiated by a particle of charge, q, undergoing an acceleration perpendicular to its direction of motion (W).
q	Particle charge (Cb).
q_e	Particle charge in units of electron charge (dimensionless).
t	Time (s).

$\vec{u}_r$	Unit vector of a cylindrical coordinate system associated with O and defining the radial direction.
$\vec{u}_\theta$	Unit vector of a cylindrical coordinate system associated with O and defining the azimuthal direction.
v_q	Modulus of $\overrightarrow{v_q}$ (m/s).
$\overrightarrow{v_q}$	Velocity vector of a particle of charge, *q*.
x	abscissa (m).
$\vec{x}$	Unit vector of a rectangular coordinate system associated with O and defining the horizontal direction.
$\vec{X}$	Unit vector of a rectangular coordinate system such that $(\Omega, \vec{X}, \vec{Z})$ defines the plane of the design orbit of an accelerator ring.
y	Ordinate (m).
$\vec{y}$	Unit vector of a rectangular coordinate system associated with O and defining the vertical direction.
$\vec{Y}$	Unit vector of a rectangular coordinate system associated with Ω, perpendicular to the plane of the design orbit of an accelerator ring.
z	*z*-coordinate (m).
$\vec{z}$	Unit vector of a rectangular coordinate system associated with O and corresponding to the main direction of particle motion.
$\vec{Z}$	Unit vector of a rectangular coordinate system such that $(\Omega, \vec{X}, \vec{Z})$ defines the plane of the design orbit of an accelerator ring.

GREEK LETTERS

$\gamma_q = 1 \Big/ \sqrt{1 - \frac{v_q^2}{c^2}}$	Lorentz factor of a relativistic particle of charge, *q* (dimensionless).
$\Delta\mathcal{E}_{GeV}$	Energy radiated by a charged particle, per revolution around a synchrotron, expressed in giga electron volts (GeV).
$\Delta\mathcal{E}_q$	Energy radiated by a particle of charge, *q*, per revolution around a synchrotron (J).
$\varepsilon_0 = 1/\mu_0 c^2 = 8.85\ 10^{-12}$ F/m	Permittivity of free space.

$\mathcal{E}_{\mathrm{GeV}}$	Total energy of a charged particle expressed in giga electron-volts (GeV).
$\mathcal{E}_{\mathrm{q}} = m_{\mathrm{q}}\,\gamma_{\mathrm{q}}\,\mathrm{c}^2$	Total energy of a charged particle of mass at rest, m_{q}, and of Lorentz factor, γ_{q} (J).
$\mathcal{E}_{\mathrm{q},0} = m_{\mathrm{q}}\,\mathrm{c}^2$	Energy at rest of a charged particle of mass at rest, m_{q} (J).
$\kappa_{\mathrm{g}} \approx 0.3\,q_{\mathrm{e}}\,g/\mathcal{E}_{\mathrm{GeV}}$	Normalized gradient of a quadrupole magnet $(\mathrm{rad/m})^2$.
$\mu_0 = 4\pi 10^{-7}$ H/m	Magnetic permeability of free space.
$\pi = 3.14159265358979323846264 3$	
τ_{q}	Revolution time of a particle of charge, q, around a synchrotron (s).
$\phi_{\mathrm{dip}} \approx l_{\mathrm{dip}} / \chi$	Angular deflection of a charged particle trajectory in a dipole magnet of length l_{dip} (rad).
$\chi \approx \dfrac{\mathcal{E}_{\mathrm{GeV}}}{0.3\,q_{\mathrm{e}}\,B}$	Bending radius of a charged particle trajectory in an uniform magnetic flux density (m).
Ω	Origin of a coordinate system associated with the design and planar orbit of an accelerator ring.

MATHEMATICAL SYMBOL

x	Vectorial product.

1 ON THE NEED OF HIGH-ENERGY ACCELERATORS

1.1 THE TOOLS OF PARTICLE PHYSICS

Nuclear and particle physics have at least two main goals: (1) studying the ultimate constituents of matter and their modes of interaction, and (2) understanding the universe origin and its early evolution [1]. The research is carried out by breaking into pieces what-are-known-to-be non-elementary particles (such as ions or protons) and by analyzing the nature and properties of the pieces. It is done also by producing interactions between what-are-thought-to-be elementary particles (such as electrons or even possibly muons) at energy levels which only existed right after the big-bang.

The tools required for such physics experiments are: (1) sources, from which the particles of interest are extracted and captured, (2) accelerators, which guide and accelerate the particles in preparation for their smashing, and (3) detectors, which surround the interaction points, and which are designed to observe and identify the interaction products. To gather statistically significant data sample, and achieve high event rates, the particles are bunched together and the bunches are formatted into high-intensity beams. Once accelerated to the desired energy level, the beam is strongly focused and blasted against a fixed target, or two beams, prepared in parallel, are brought into head-on collisions.

1.2 BRIEF HISTORY OF PARTICLE ACCELERATORS

The only particles we know how to capture, guide and accelerate are charged particles, and this is done by means of strong electromagnetic fields.

The principles of modern particle accelerators were developed and demonstrated by Ernest O. Lawrence and his Ph.D. student, M. Stanley Livingston, who, in 1931, built the first *cyclotron* at the University of California at Berkeley. This proof-of-principle device relied on a conventional magnet whose pole faces were a little less than 10 cm in diameter and was able to accelerate hydrogen-molecule ions to about 80 keV (1 eV $\approx$ 1.6 10^{-19} J) [2]. Soon after, the pair, helped by David Sloane, built a second and larger device, relying on an electromagnet with 11-inch (27.9-cm) diameter pole faces, shown in Figure 1, and which, in January 1932, accelerated protons up to 1.22 MeV [3]. The invention of the cyclotron earned E.O. Lawrence the Nobel prize in Physics in 1939.

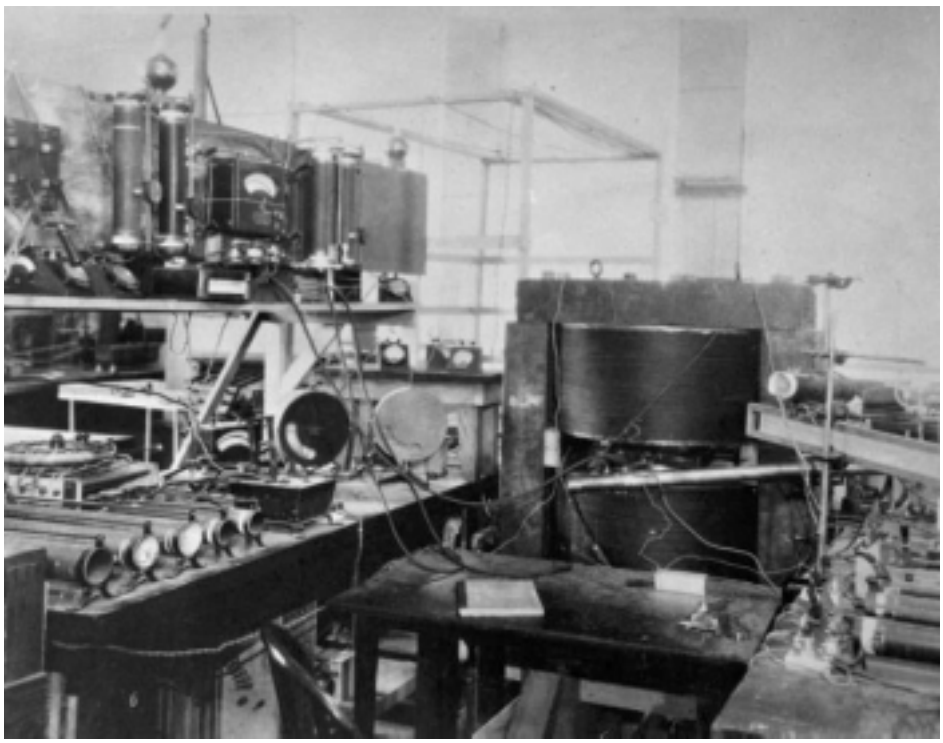

Figure 1. View of the 11-inch cyclotron built by E.O. Lawrence, *et al.*, and which, in January 1932, accelerated protons up to 1.22 MeV.

Since then, a large number of machines have been built and operated around the world. Countless technological innovations on their various components (from sources to accelerators and detectors) have led to regular performance improvements and to a long stream of Nobel-prize-winning discoveries in nuclear and particle physics. Today's giant machines exceed the kilometric scale and accelerate electron and positron beams up to 100 GeV (1 GeV $\approx 10^9$ eV) and proton and anti-proton beams up to about 1 TeV (1 TeV $\approx 10^{12}$ eV). (Note that since protons are not elementary, they have to be accelerated to higher momenta than electrons to achieve similar interaction energies at the level of their constituents.)

1.3 PERSPECTIVES

In spite of the spectacular achievements mentioned above, there is still a strong push to probe deeper and deeper into the heart of matter and to go back closer and closer to the big bang. This means a further increase in particle energy and/or a bolstering of the interaction rates to improve statistics. The next generation of machines, presently under design or construction, calls for electron beams of 500 GeV or more and for proton beams in excess of 5 TeV. Some are even dreaming of a proton machine delivering 50 TeV per beam. Hence, the development of high-energy accelerators is not yet at an end, and although the size and costs of the machines have reached critical levels, one can expect, for the next 10 to 20 years, the work on accelerator technologies to be as vigorous as ever.

2 HIGH-ENERGY ACCELERATOR TYPES

2.1 CLASSIFICATION

Nowadays, there are two main types of high-energy particle accelerators: (1) linear accelerators, referred to as *LINACs*, and (2) circular accelerators, referred to as *synchrotrons*. Synchrotrons are the large-scale successors of the cyclotrons, pioneered by Lawrence in the 1930's, whose concepts appeared to be ill suited for energies beyond a few hundreds of MeV per unit of atomic mass [4].

2.2 LINEAR ACCELERATORS

The principle of a linear accelerator is to let the bunches of charged particles travel once through the machine along a mostly straight trajectory. This offers at least two main advantages: (1) it only requires a limited number of trajectory-bending elements and (2) the level of electromagnetic radiations emitted by the accelerating particles is low. It has two main disadvantages: (1) the particle bunches cannot be re-circulated and (2) the achievement of high momenta requires a large number of accelerating stations positioned one after the other along the particle trajectories.

As of today (2000), the longest and most powerful linear accelerator is that of the Stanford Linear Collider (SLC), implemented at the Standford Linear Accelerator Center (SLAC), near Palo Alto, California. The SLC LINAC, shown in Figure 2, is 2 miles (3.2 km) long and is capable of accelerating electron and positron beams up to 50 GeV.

2.3 CIRCULAR ACCELERATORS

The principle of a circular accelerator, also referred to as *accelerator ring*, is to circulate the particle beam many times around a closed orbit. This offers at least two advantages: (1) the particle bunches can be accumulated and stored in the accelerator ring and (2) it only requires a few accelerating stations, through which the particles go at every turn. It has two main disadvantages: (1) it calls for a large number of trajectory-bending elements distributed over the ring arcs and (2) the level of radiations emitted by the rotating particles, referred to as *synchrotron radiation*, can be very high, especially for light particles such as electrons (see section 3.5).

Until November 2000, the largest circular accelerator in operation was the Large Electron Positron (LEP) collider, implemented at the European Laboratory for Particle Physics (CERN). As illustrated in Figure 3 (and described in section 2.5), it had a circumference of 27 km and was capable of accelerating electron and positron beams up to 100 GeV.

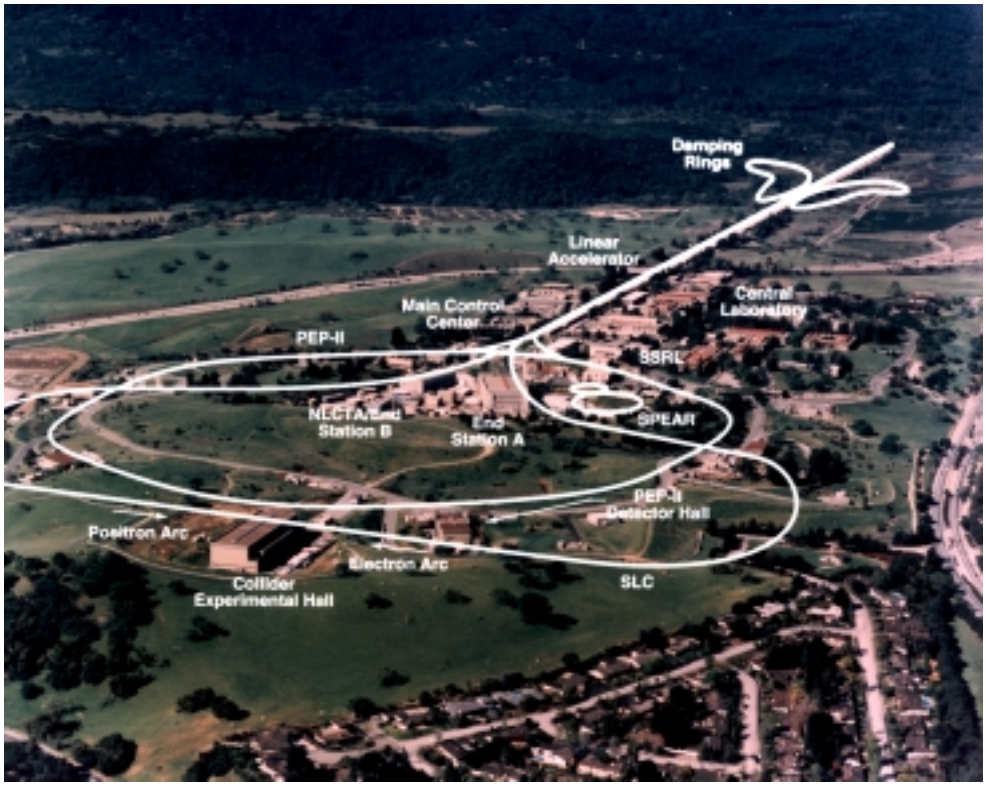

Figure 2. Aerial view of the SLAC accelerator complex.

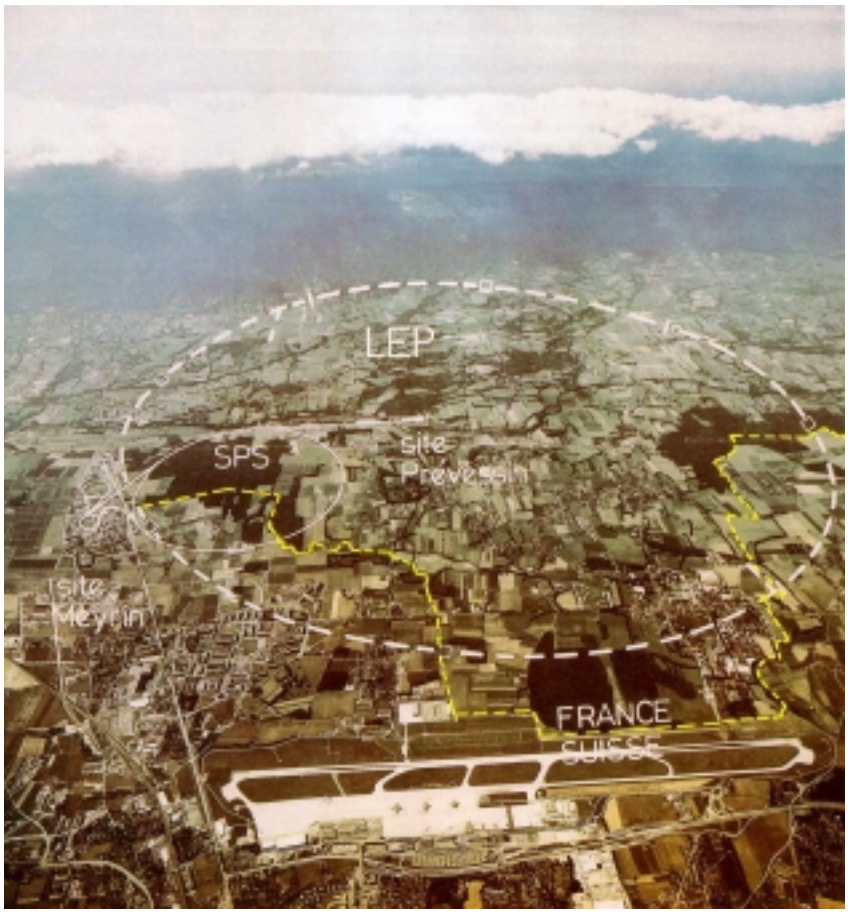

Figure 3. Aerial view of the CERN accelerator complex. The scale is given by Geneva airport at the figures's bottom.

2.4 ACCELERATOR COMPLEX AND COLLIDER

The most powerful machines are made up of several stages, which progressively raise the beam energy. Each stage is a fully-fledged accelerator, which can be of either type. The beam, prepared in the accelerator chain, is then used to produce interactions.

A collider is a machine where two beams are prepared in parallel, either in linear or in circular accelerators, and are brought into head-on collisions at the last stage. This offers the advantage of doubling the interaction energy in a reference frame tied up to the center of mass of the colliding particles.

2.5 EXAMPLE: CERN FACILITY

The CERN facility, depicted in Figure 3, is located at the French/Swiss border near Geneva, Switzerland. In addition to several linear accelerators, four circular machines have been built and operated over the years: (1) the Proton Synchrotron Booster (PSB), (2) the Proton Synchrotron (PS), (3) the Super Proton Synchrotron (SPS), and (4) the Large Electron Positron (LEP) collider.

The Proton Synchrotron Booster has a 50-m diameter and can accelerate protons up to 1 GeV (1 GeV $\approx$ 1.6 10^{-10} J). The Proton Synchrotron has a 200-m diameter. It was commissioned in November 1959 and can accelerate protons up to 26 GeV. The Super Proton Synchrotron has a circumference of 6.9 km and is installed in an underground tunnel at a depth varying from 25 to 65 m. It was commissioned in September 1976 and can raise the proton energy up to 450 GeV.

As mentioned above, until recently, the largest ring of the CERN complex was the LEP collider, installed in an underground tunnel, at a depth varying from 50 to 150 m, and with a 27 km circumference [5]. The LEP collider was commissioned in July 1989 and was operated as an electron/positron collider with energy of about 100 GeV per beam. It was switched off definitely on November 2, 2000, and will be dismantled in the course of 2001.

The LEP beams were designed to collide at four interaction points surrounded by four experiments: ALEPH (standing for Apparatus for LEP PHysics), DELPHI (standing for DEtector with Lepton, Photon and Hadron Identification), L3, and OPAL (standing for Omni-Purpose Apparatus at LEP). Figure 4 shows a view of the ALEPH experiment, which included a large superconducting solenoid, embedded in the detector array. This solenoid was designed and built at Commissariat à l'Energie Atomique de Saclay (CEA/Saclay), near Paris, France [6]. It was 7 m long, had a 5 m inner bore, and produced a 1.5 T central field. The stored energy was 140 MJ and the total weight of the cold mass was 25 metric tons.

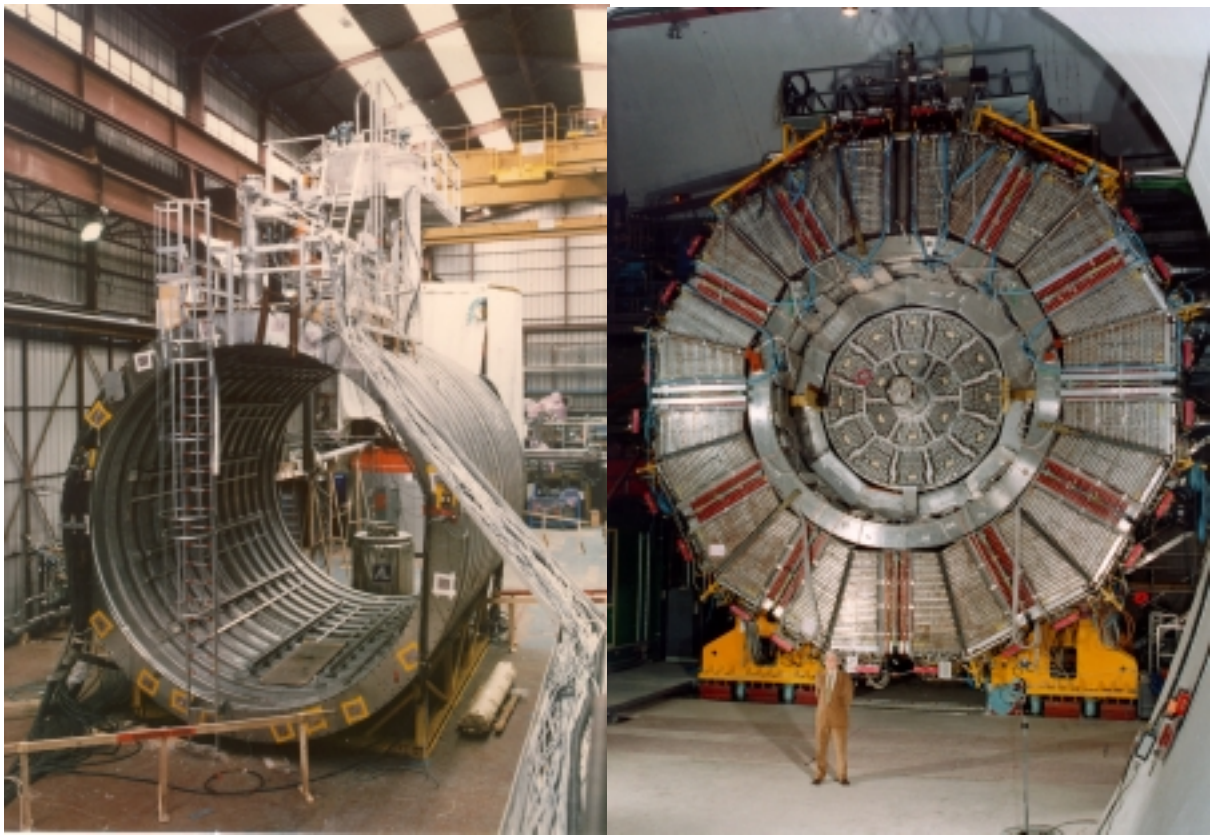

Figure 4. Views of the superconducting solenoid ALEPH, implemented in one of the LEP collider experiments at CERN: (a) under tests at CEA/Saclay (left), and (b) surrounded by the detector array at the bottom of the CERN cavern (right; at the picture's foreground is Jack Steinberger, Nobel Laureate in Physics, 1988 –with Leon Lederman and Melvin Schwartz– for the discovery of the muon neutrino).

In December 1994, CERN has approved the construction in the existing 27 km long tunnel of the Large Hadron Collider (LHC). LHC will be a proton-proton collider with a maximum energy of 7 TeV per beam that will replace the LEP ring and that will use the PSB, PS and SPS as injector chain. Salient LHC parameters, extracted from the so-called *yellow book* [7], are summarized in Table 1 and detailed descriptions of the machine and of the planned high energy physics experiments are given in section 4.6. Commissioning is scheduled for 2005.

3 SYNCHROTRON-TYPE ACCELERATORS

3.1 ACCELERATOR MAIN RING

In this review, we only consider accelerator chains whose last stage is a closed-orbit ring, to which we shall refer as *main ring*. In the largest machines, the main ring is usually installed in an underground tunnel and, as in the case of LEP at CERN, its circumference can exceed 10 kilometers.

Table 1. Salient parameters of the Large Hadron Collider (LHC) at CERN [7].

	Injection	Storage/Collision
Layout		
Total circumference (m)	26658.883	
Number of arcs	8	
Bending radius (m)	2784.32	
Number of insertion regions	8	
Insertion region length (m)	528	
Number of interaction points	4	
Beam energy (GeV)	450	7000
Arc magnet lattice		
Number of cells per arc	23	
Cell length (m)	106.92	
Number of twin-aperture dipole magnets per cell	6	
Number of twin-aperture quadrupole magnets per cell	2	
Twin-aperture arc dipole magnet		
Total number	1232	
Magnetic length (m)	14.300	
Dipole field strength (T)	0.539	8.386
Twin-aperture arc quadrupole magnet		
Total number	386	
Magnetic length (m)	3.10	
Quadrupole field gradient (T/m)	14.5	223

The main ring of an accelerator chain is operated in three phases: (1) *injection*, during which the beam, which has been prepared in various pre-accelerators, is injected at low energy, (2) *acceleration*, during which the beam is accelerated to nominal energy, and (3) *storage*, during which the beam is circulated at nominal energy for as long as possible and is made available for physics experiments. As mentioned in section 1.1, there are two types of experiments: (1) *fixed-target* experiments, for which the beam is extracted from the main ring to be blasted against a fixed target, and (2) *colliding-beam* experiments, for which two counter-rotating beams are blasted at each other. In either case, the breakage products are analyzed in large detector arrays surrounding the targets or collision points.

An accelerator main ring includes a small series of accelerating elements, located in one ring section, and through which the charged particles go at every turn. It includes also a large number of guiding elements, which are distributed over the ring arcs. These elements must all work in synchronization to ensure that the beam orbit remains the same throughout injection, acceleration and storage [8], [9]. This explains the denomination of *synchrotron* that is used to describe this type of machines.

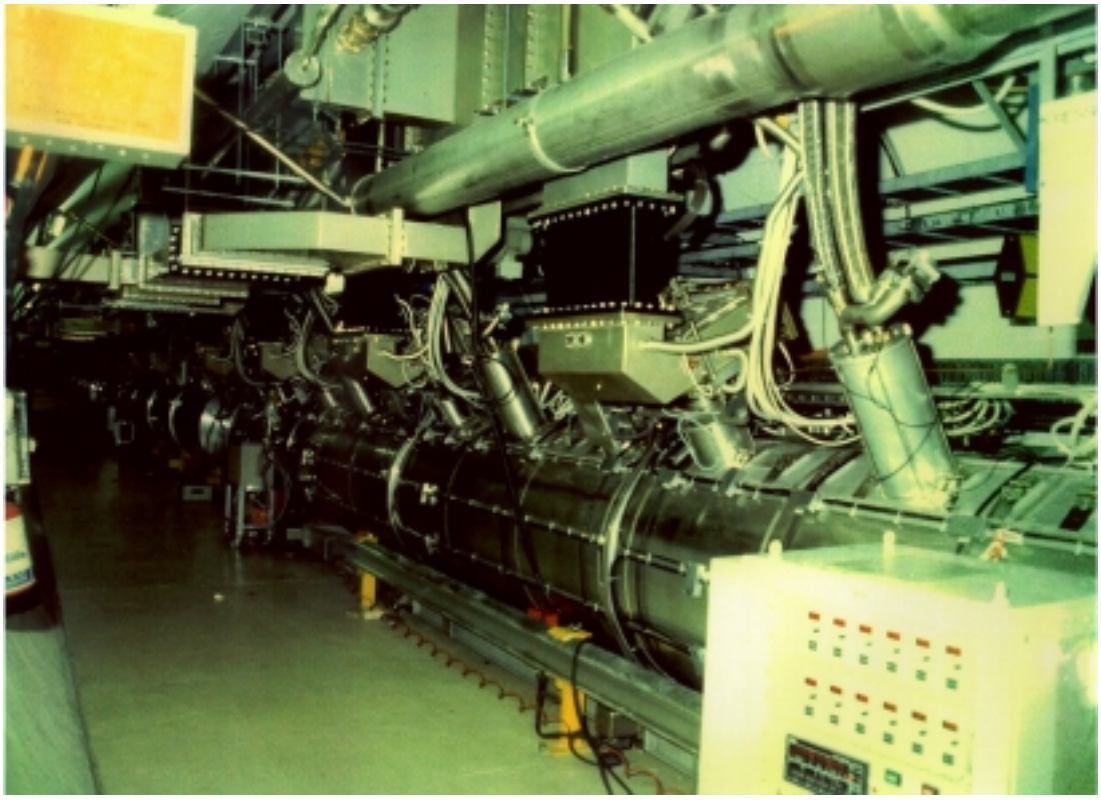

Figure 5. View of a set of superconducting RF cavity modules used in the LEP collider at CERN.

3.2 CHARGED PARTICLE ACCELERATION

Charged particles are accelerated by means of electric fields. The force, $\vec{F}_C$, exerted by an electric field, $\vec{E}$, on a charge, *q*, is given by Coulomb's law

$$\vec{F}_C = q\,\vec{E} \tag{1}$$

Such a force results in acceleration parallel to $\vec{E}$.

In most particle accelerators, the accelerating stations are made up of Radio Frequencies (RF) cavities, which can be either normal conducting or superconducting [10]. Figure 5 shows a set of superconducting RF cavity modules used for the LEP collider [11]. The 12.5-m-long modules included four cavities made up of four half-wavelength, quasi-spherical cells. The cavities were operated at a frequency of 352.209 MHz and a nominal average electric field of 6 MV/m. LEP relied on 272 superconducting cavities, providing a nominal RF voltage of about 2800 MV (corresponding to an active length of 462 m).

LHC will rely on two separate RF systems (one for each beam) designed to provide a maximum RF voltage of 16 MV per beam. Each system will be made up of 8 single-cell, superconducting cavities, operated at 400.8 MHz and delivering a nominal average electric field of 5.3 MV/m. The cavities will be grouped by four in 6.5-m-long modules.

It is worth mentioning that average electric fields of 25 MV/m are now routinely achieved in 9-cell, 1.3 GHz superconducting RF cavities developed as part of the R&D efforts for the Tera Electron volts Superconducting Linear Accelerator (TESLA) [12]. TESLA is an electron/positron linear collider, with energy of 500 GeV per beam, under consideration at the Deutsches Elektronen-SYnchrotron (DESY), near Hamburg, Germany [13].

3.3 CHARGED PARTICLE GUIDING AND FOCUSING

Beams of charged particles are guided and focused by means of magnetic flux densities. The force, $\overrightarrow{F_L}$, exerted by a magnetic flux density, $\vec{B}$, on a charge, q, traveling at a velocity, $\overrightarrow{v_q}$, is given by Lorentz' law

$$\overrightarrow{F_L} = q\, \overrightarrow{v_q} \times \vec{B} \tag{2}$$

Such a force is perpendicular to the directions of $\overrightarrow{v_q}$ and $\vec{B}$ and its only action is to bend the particle trajectory.

If $\overrightarrow{v_q}$ and $\vec{B}$ are perpendicular, the particle is deviated on an arc of a circle, tangent to $\overrightarrow{v_q}$ and perpendicular to $\vec{B}$, whose radius of curvature, χ, can be estimated as

$$\chi = \frac{m_q\, \gamma_q\, v_q}{q\, B} \tag{3}$$

Here, m_q is the particle mass at rest, v_q and B are the amplitudes of $\overrightarrow{v_q}$ and $\vec{B}$, and γ_q is the relativistic Lorentz factor defined as

$$\gamma_q = \frac{1}{\sqrt{1-\frac{v_q^2}{c^2}}} \tag{4}$$

where c is the speed of light.

Assuming that the particle total energy, $\mathcal{E}_q = m_q\, \gamma_q\, c^2$, is far greater than its energy at rest, $\mathcal{E}_{q,0} = m_q\, c^2$, Eq. (3) can be recast in the form

$$\chi \approx \frac{\mathcal{E}_q}{c\, q\, B} \approx \frac{\mathcal{E}_{GeV}}{0.3\, q_e\, B} \tag{5}$$

where χ is in meters, B is in teslas, q_e is the particle charge in units of electron charge, and $\mathcal{E}_{GeV}$ is the particle total energy expressed in giga electron volts (GeV).

Figure 6. View of the conventional electromagnet ring of the LEP collider at CERN.

Equation (5) shows that, to maintain a constant radius of curvature as the particle is accelerated, B must be ramped up linearly with $\mathcal{E}_{\mathrm{GeV}}$, which is one of the operating principles of a synchrotron.

In circular machines, the magnetic flux densities are provided by electromagnets distributed around the ring. Figure 6 shows a view of the conventional electromagnet ring of the LEP collider at CERN (that will be dismantled in 2001 to leave room for LHC).

3.4 BEAM ENERGY VERSUS BENDING RADIUS

Let us use Eq. (5) to dimension a 10 TeV proton accelerator, choosing successively for B, a low value of 2 T, an intermediate value of 6 T, and a high value of 10 T. The results are presented in Table 2. The computed bending radii go from 3.3 km (high-field option) to 16.7 km (low-field option). This shows that, when designing a large synchrotron-type accelerator, a trade-off must be found between, on one hand, the availability of land and the tunneling costs, and, on the other hand, the feasibility and costs of the electromagnets.

For LHC at CERN, the radius of curvature of the existing LEP tunnel limits the χ-value. In the yellow book design, χ is worth 2784.32 m and the magnetic flux density of the bending magnets in the storage/collision phase is set to 8.386 T (see Table 1). With c = 299 792 458 m/s, it follows from Eq. (5) that the maximum proton energy is 7000 GeV.

Table 2. Bending radius for a 10-TeV proton accelerator.

	B (T)	χ (km)
Low Field	2	16.7
Medium Field	6	5.6
High Field	10	3.3

3.5 SYNCHROTRON RADIATION

Let us consider a particle of charge, q, undergoing an acceleration, a_q, perpendicular to its direction of motion. This particle, radiates a power, P_q, which, in the laboratory frame, can be estimated as [9]

$$P_q = \frac{1}{6\pi\varepsilon_0} \frac{q^2 a_q^2}{c^3} \gamma_q^4 \tag{6}$$

where ε_0 is the permittivity of free space, c is the speed of light, and γ_q is the relativistic Lorentz factor defined by Eq. (4).

If we assume, as in the case of a particle describing the design orbit of a synchrotron, that the perpendicular acceleration corresponds to a centripetal acceleration on a trajectory of bending radius, χ, we can write

$$a_q \approx \frac{v_q^2}{\chi} \tag{7}$$

where v_q is the particle velocity.

If we further assume, as in section 3.3, that the particle total energy, $\mathcal{E}_q = m_q \gamma_q c^2$, is far greater than its energy at rest, $\mathcal{E}_{q,0} = m_q c^2$ (where m_q is the particle mass at rest), the combination of Eqs. (4), (6) and (7) yields

$$P_q \approx \frac{1}{6\pi\varepsilon_0} \frac{q^2}{m_q^4 c^7} \frac{\mathcal{E}_q^4}{\chi^2} \tag{8}$$

The above equation shows that the radiated power varies like the fourth power of the particle total energy and is inversely proportional to the fourth power of the particle mass at

rest. It appears also that, for a given $\mathcal{E}_q$ value, massive particles, such as protons, radiate far less power than light particles, such as electrons.

Furthermore, for a particle whose velocity is near that of light, the revolution time, τ_q, can be estimated as

$$\tau_q \approx \frac{2\pi\chi}{c} \tag{9}$$

By combining Eqs. (8) and (9), it follows that the energy loss per turn, $\Delta\mathcal{E}_q$, is

$$\Delta\mathcal{E}_q \approx \frac{1}{3\varepsilon_0} \frac{q^2}{m_q^4 c^8} \frac{\mathcal{E}_q^4}{\chi} \tag{10}$$

The above equation can be rewritten as

$$\Delta\mathcal{E}_{GeV} \approx 88.510^{-6} \frac{q_e^2 \mathcal{E}_{GeV}^4}{m_e^4 \chi} \tag{11}$$

where q_e is the particle charge in units of electron charge, m_e is the particle mass at rest in units of electron mass at rest, and $\mathcal{E}_{GeV}$ and $\Delta\mathcal{E}_{GeV}$ are the particle total energy and the energy loss per turn expressed in giga electron volts (GeV).

In the case of LEP [5]: $m_e = q_e = 1$, and $\chi = 3096.175$ m. Taking $\mathcal{E}_{GeV} = 100$, we get

$$\Delta\mathcal{E}_{GeV} \approx 2.9 \text{ GeV} \tag{12}$$

The energy loss per turn is quite large and must be compensated by the RF system. As indicated in section 3.2, the LEP RF voltage was designed to be 2.8 GV. It turned out, however, that the performances of the installed, superconducting RF cavities exceeded the design values (with an average electric field over the total cavity production of about 7.5 MV/m compared to the required 6 MV/m). As a result, center-of-mass energies as high as 209 GeV have been achieved in April 2000 [14]. In spite of this record, LEP is likely to be the largest circular electron machine ever built.

In the case of LHC: $q_e = 1$, $m_e = 1836.1$, and $\chi = 2784.32$ m. Taking $\mathcal{E}_{GeV} = 7000$, we get

$$\Delta\mathcal{E}_{GeV} \approx 6.7 \text{ keV} \tag{13}$$

Even though the energy is 70 times greater than for LEP, the proton mass at rest is so much greater than the electron mass at rest that the energy loss per turn is reduced by a factor 430000.

For a machine such as LHC, the dimensioning of the RF system is not driven by concerns about energy loss per turn. It remains, however, that given the large number of particles stored in the ring, the power issued from this type of radiation, referred to as *synchrotron radiation*, becomes quite sizeable (of the order of 0.2 W/m per beam [7]) and must be evacuated to avoid heating of superconducting magnet coils.

4 LAYOUT OF LARGE CIRCULAR ACCELERATORS

4.1 MAGNET CLASSIFICATION

The main ring of an accelerator chain is usually made up of several *bending arcs* separated by quasi-straight *insertion regions*. The bending arcs have the same radius of curvature and are designed to provide an integrated bending angle of (2π). The insertion regions house the accelerating stations and the beam injection and extraction lines. In the case of a collider ring, the two counter-rotating beams are designed to cross at the middle of at least one of the insertion regions. The insertion region middle points where the beams cross are referred to as *interaction points* and the space around them is available for experiments.

The electromagnets found around an accelerator main ring can be classified into four categories: (1) a large number of *arc magnets*, distributed over the ring arcs, (2) a limited number of *insertion* and *final focusing magnets*, used to handle the beams in the insertion regions and near the targets or collision points, (3) a large number of *corrector magnets*, associated with both arc and insertion magnets, and (4) large *detector magnets* implemented in the physics experiments.

4.2 ARC MAGNETS

The magnets distributed over the ring arcs have two main functions: (1) bending of the beam around a closed and constant orbit, and (2) focusing of the beam to achieve a proper size and intensity. In large machines, the bending and focusing functions are separated: the former is provided by dipole magnets whereas the latter is provided by pairs of focusing/defocusing quadrupole magnets (see section 5.3). These magnets are arranged around the arcs in a regular lattice of cells, made up of a focusing quadrupole, a string of bending dipoles, a defocusing quadrupole and another string of bending dipoles [15]. Due to their large number, the arc magnets are usually mass-produced in industry.

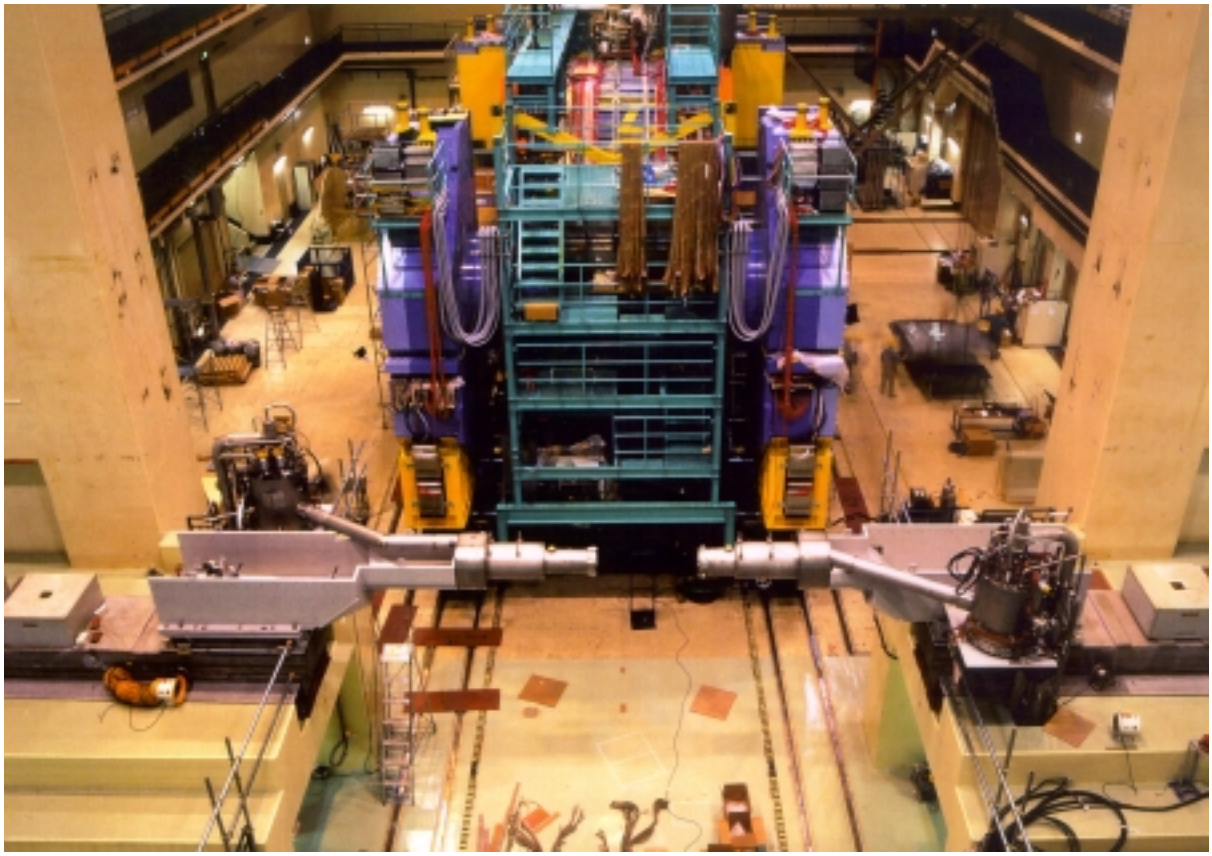

Figure 7. Implementation of the final focusing quadrupole magnets for the KEK-B factory. The magnets are shown in front of the BELLE detector, which has been railed back from its normal position.

4.3 INSERTION AND FINAL FOCUSING MAGNETS

A number of special magnets are required to transport the beam from the injector chain to the main ring and to handle the beam in the insertion regions. Among them are sets of strongly focusing quadrupole magnets located near the targets or collision points. The design and fabrication of the insertion and final focusing magnets are very similar to those of the arc magnets, except that they are produced in limited series and that they have to be customized to their crowded environment.

It is worth mentioning that, in some cases, the beam optics requirements are such that the final focusing quadrupole magnets end up at the extremities or even inside the physics experiment and must be designed to sustain the stray field of the detector magnet (if any). This is illustrated in Figure 7, which shows the implementation of the superconducting quadrupole magnets for the interaction region of the KEK-B factory [16]. The magnets are presented in front of the BELLE detector, which has been railed back from its normal position. The KEK-B factory is a two-ring machine built at KEK, High Energy Accelerator Research Organization, near Tsukuba, Ibaraki prefecture, Japan, that is designed to collide a 8 GeV electron beam with a 3.5 GeV positron beam at a single interaction point [17].

4.4 CORRECTOR MAGNETS

A large number of corrector magnets are needed to compensate, either locally or globally, the alignment errors and the field quality errors of the main magnets. Some of them are dedicated also to special functions required for fine-tuning of beam optics.

The corrector magnets can be more numerous than the arc magnets, but are usually small in size and cost, and have low performance requirements. In big machines, most of them are superconducting and are mounted inside the cryostats of the main magnets. As for the arc magnets, the large series are mass-produced in industry.

4.5 DETECTOR MAGNETS

The physics experiments surrounding the targets or collision points usually rely on large magnet systems, which are embedded in the detector, array [18]. The magnet system is based either on a solenoid or on a toroid (or on a combination of both; see section 6). The magnet structure must be minimized to save space and to reduce interactions with the particles. Furthermore, once buried in the detector array, the magnet system is no longer accessible for repair and maintenance and, therefore, must be engineered to operate safely and reliably. The technology of detector magnets is very different from that of accelerator magnets and is not discussed in this review.

4.6 EXAMPLE: LHC AT CERN

4.6.1 LAYOUT

As an illustration, Figure 8 shows the layout of LHC at CERN [7]. The LHC ring is divided into 8 bending arcs separated by 8 insertion regions, designated as IR1 through IR8. The ring circumference is 26658.883 m and each insertion region is about 528 m long (see Table 1). The two counter-rotating proton beams circulate around the eight arcs and cross at the middle of four of the insertion regions. Two of these crossings, located diametrically opposite in the ring, are designed to achieve high interaction rates. The corresponding insertions, IR1 and IR5, are referred to as *high-luminosity* insertions and house the main physics experiments (ATLAS and CMS). The insertions where the two other crossings take place, IR2 and IR8, are referred to as *low-luminosity* insertions. They contain the injection systems and will be used for other experiments (ALICE and LHC-B). The accelerating stations, described in section 3.2, are located in one of the insertion regions where the beams do not cross (IR4). IR3 and IR7 house beam cleaning systems, while IR6 includes a beam dumping system to abort safely the beam at the end of physics runs.

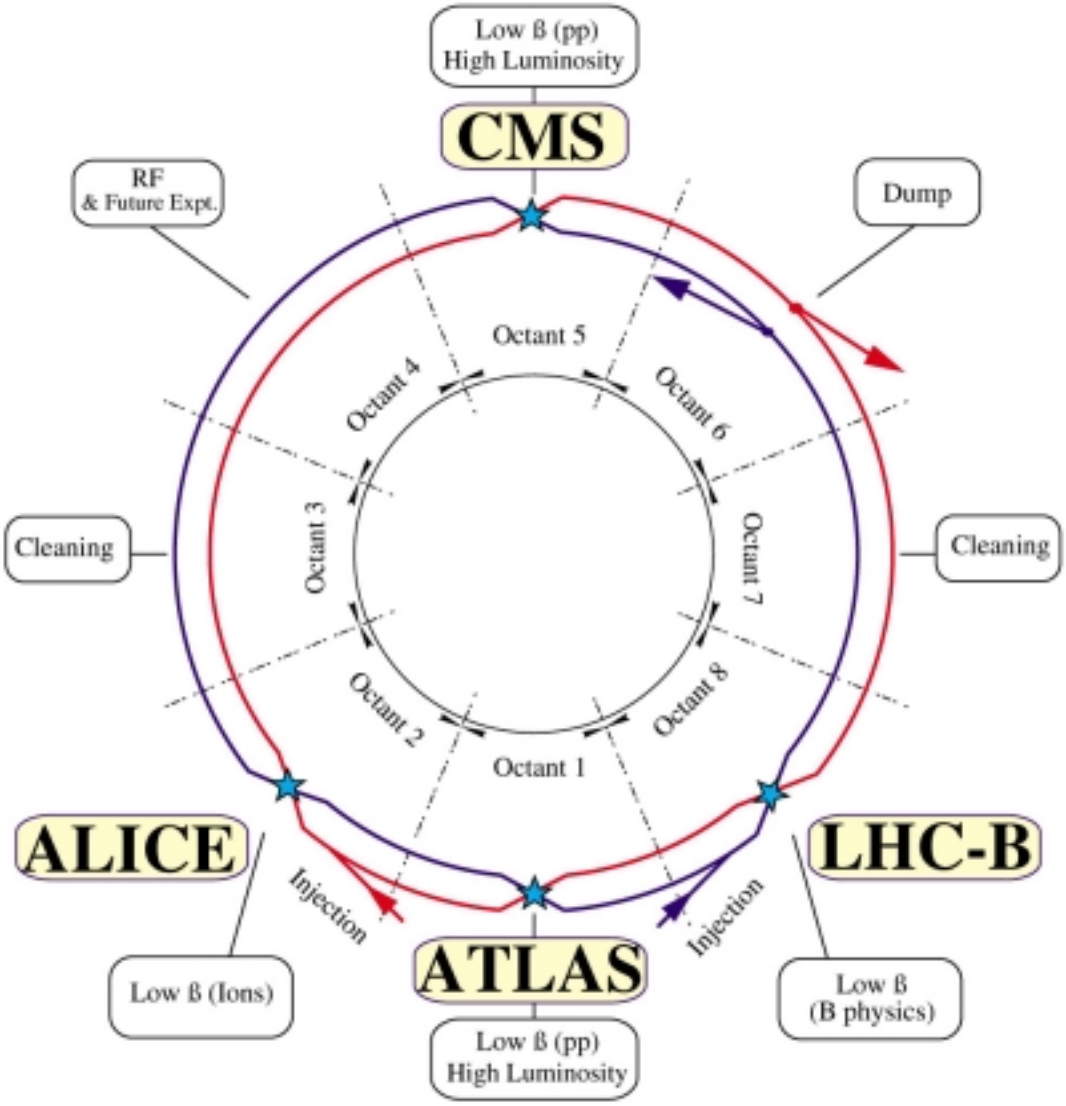

Figure 8. Schematic layout of the Large Hadron Collider (LHC) at CERN.

4.6.2 LHC ARCS

The 8 bending arcs of LHC have identical magnet lattices. They include 23 cells, which, as represented in Figure 9, are made up of 6 superconducting dipole magnets, 1 focusing and 1 defocusing quadrupole magnet, also superconducting, and several corrector magnets. The arc dipole and quadrupole magnets are mounted in individual cryostats and are operated at 1.9 K. Both magnet types have two 56-mm apertures, housing pipes for the counter-rotating proton beams. Such magnet design is referred to as *twin aperture*, and the distance between the central axes of the two apertures is 194 mm. The arc dipole magnets are 14.3 m long and are designed to produce a magnetic flux density of 8.386 T during the storage/collision phase. The arc quadrupole magnets are 3.1 m long and are designed to operate with a maximum field gradient of 223 T/m. The cell length is 106.9 m.

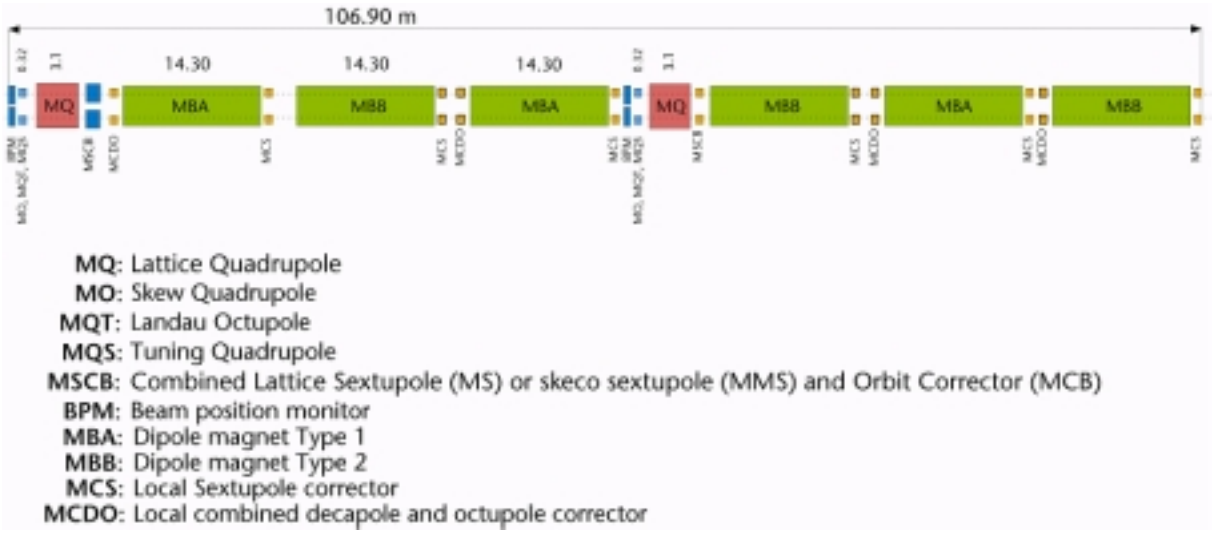

Figure 9. Cell of the proposed magnet lattice for LHC arcs at CERN.

4.6.3 LHC INSERTION REGIONS

In the four insertion regions where the two beams cross, two sets of special magnets are required: (1) dipole magnets, to bring the beams together on one side of the collision points and to separate them on the other side, and (2) quadrupole magnets, to ensure final focusing on both sides of the collision points.

Figure 10 shows the proposed magnet lattice on the right hand-side of one of the low-luminosity collision points. Starting from the interaction point and moving away from it, we find [19]: (1) a so-called *inner triplet* of single-aperture quadrupole magnets, (2) two so-called *separation/recombination* dipole magnets (a single-aperture one, followed by a twin-aperture one), and (3) a so-called *matching section* of four twin-aperture quadrupole magnets (note that only two of those are depicted). The lattice on the other side of the interaction point includes similar sets of magnets, with some variants to accomodate beam injection.

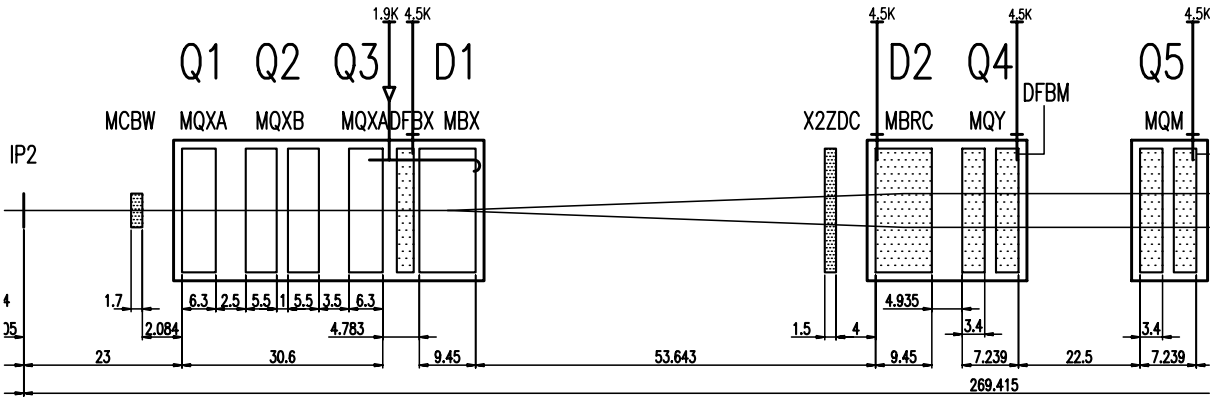

Figure 10. Proposed magnet lattice for the right-hand side of one of the low luminosity interaction points of LHC at CERN.

The inner triplet is made up of four, superconducting, high-field-gradient quadrupole magnets, grouped into three different cryostats and operated at 1.9 K. These magnets, with lattice designation Q1, Q2a, Q2b and Q3, have one, 70-mm aperture, and accommodate the two beams within a single pipe. They are powered in series by a common power supply. (Note that Q1 and Q2 are focusing while Q2a and Q2b are defocusing –see section 5.3).

The beam separation is performed in two stages: (1) a first 4-T, single-aperture dipole magnet, with lattice designation D1, handles the beams exiting from the inner triplet into a single, large beam pipe, and (2) a second 4-T, twin-aperture dipole magnet, with lattice designation D2, located somewhat further away from the collision point, handles the beams exiting from D1 into two separate beam pipes. The D1 magnets implemented in the high-luminosity insertions are resistive (because of large beam losses), while those implemented in the low-luminosity insertions are superconducting. The D2 magnets are all superconducting, and the distance between the central axes of their two apertures is 188 mm.

Furthermore, additional superconducting dipole magnets are required in the insertion region where the accelerating stations are located. These magnets, with lattice designation D3a, D3b, D4a and D4b, are used to increase the beam separation from 194 mm to 420 mm at one end of the stations and to bring it back to 194 mm at the other end, so that dedicated RF cavity modules can be installed on each of the beam lines. The magnetic lengths of the superconducting D1, D2, D3 and D4 dipole magnets is 9.45 m and the inner bore diameter of the coil assemblies is 80 mm. Magnets D1, D4a et D4b are operated at 1.9 K, while magnets D2, D3a and D3b are operated at 4.5 K.

The matching section is made up of several twin-aperture quadrupole magnets, grouped into four different cryostats, with lattice designations Q4, Q5, Q6 and Q7. Most of them are individually powered and have standard, 56-mm apertures, but a few (Q4 and Q5 in the low-luminosity insertions) require larger, 70-mm apertures.

4.6.4 LHC EXPERIMENTS

At present (2000), two high-energy physics experiments are being developed for LHC: (1) ATLAS (which stands for Air core Toroid for Large Acceptance Spectrometer or A Toroidal LHC ApparatuS), and (2) CMS (which stands for Compact Muon Solenoid). Both experiments rely on large magnet systems, which are embedded in the detector array. Salient parameters of these magnets, which are engineered at various laboratories around the world under CERN supervision, are summarized in Table 3.

Table 3. Salient parameters of superconducting magnets for LHC experiments at CERN.

Experiment Magnet Name Reference	ATLAS Barrel Toroid [20]	ATLAS End Cap Toroids [24]	ATLAS Central Solenoid [21]	CMS Solenoid [26]
Developer(s)	CEA/Saclay & INFN/Milan	RAL	KEK	CEA/Saclay INFN/Genoa & ETH
Number of coils	8	2 x 8	1	1
Length (m)	25.3	5	5.3	12.5
Inner diameter (m)	9.4	1.65	2.468	6.320
Outer diameter (m)	20.1	10.7	2.63	6.944
Operating Current (kA)	20.5	20.0	7.6	19.5
Central field (T)			2.0	4.0
Maximum field on coil (T)	3.9	4.13	2.6	4.6
Stored energy (MJ)	1080	2 x 250	39	2670

As shown in Figure 11, the magnet system for ATLAS is made up of four superconducting elements [20]: (1) a Central Solenoid (CS), located at the detector heart and providing a 2.0-T axial magnetic flux density, (2) a Barrel Toroid (BT), located around the central solenoid, and (3) two End-Caps Toroids (ECT), inserted at both ends of the Barrel Toroid and lined up with the Central Solenoid.

The Central Solenoid is engineered at KEK [21]. It is 5.3 m long with a 2.3 m free bore inner diameter. The stored energy is 39 MJ and the peak magnetic flux density on the conductor is 2.6 T. The Barrel Toroid was initially designed at CEA/Saclay [22], and is now developed by a collaboration including CEA/Saclay and the Istituto Nazionale di Fisica Nucleare, Sezione di Milano (INFN/Milan), in Italy [23]. It is made up of 8 racetrack-type coils, with an overall length of 25.3 m. The Barrel Toroid inner diameter is 9.4 m and its outer diameter is 20.1 m. The total (8 coils) stored energy is 1.1 GJ and the peak magnetic flux density on the conductor is 3.9 T. The two End-Cap Toroids are also made up of 8 racetrack-type coils, with an overall length of 5 m. The End-Cap Toroids' inner radii are 1.65 m and their outer radii are 10.7 m. The stored energy is 250 MJ per toroid and the peak magnetic flux density on the conductor is 4.13 T. The End-Cap Toroids are engineered at Rutherford Appleton Laboratory (RAL) in the United Kingdom [24]. The overall length of the ATLAS experiment is 44 m, while its overall diameter is 22 m.

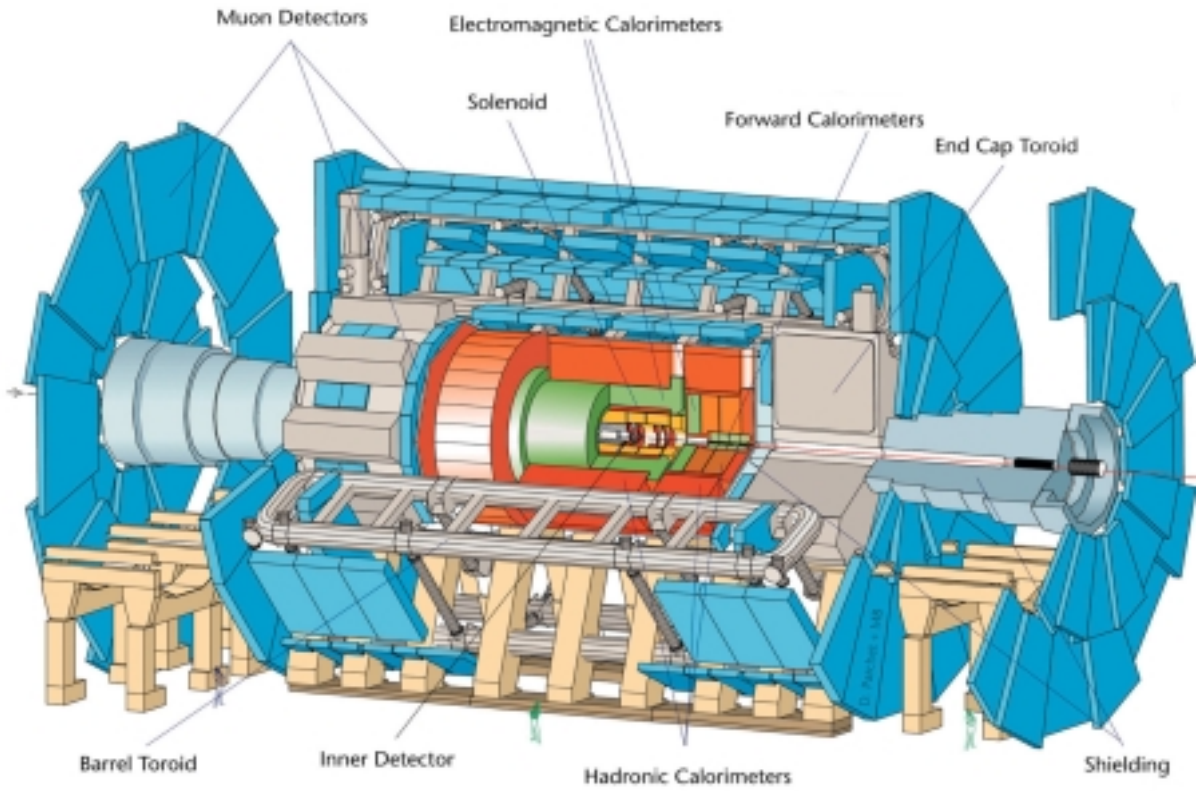

Figure 11. Artist view of the proposed ATLAS experiment for LHC at CERN.

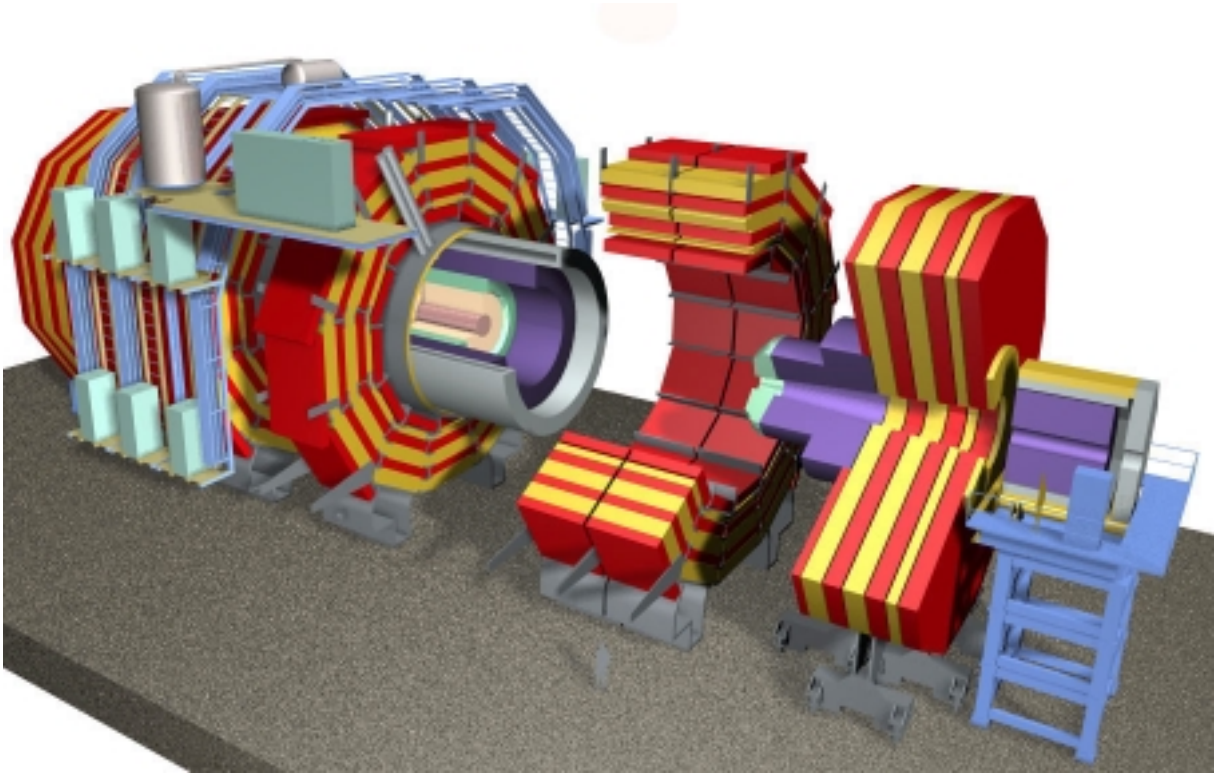

Figure 12. Artist view of the magnetic system for the proposed CMS experiment at CERN showing the superconducting solenoid at the heart of its iron yoke.

As illustrated in Figure 12, the magnetic system for the CMS detector is made up of a large superconducting solenoid surrounded by an iron yoke. The superconducting solenoid is 12.5 m long with a 5.9 m free bore inner diameter. It produces an axial magnetic flux density of 4.0 T. The stored energy is 2.7 GJ and the peak magnetic flux density on the conductor is 4.6 T. Similarly to the ATLAS Barrel Toroid, the CMS solenoid was initially designed at CEA/Saclay [25], and is now developed by a collaboration including CEA/Saclay and INFN/Genoa, along with the Swiss Federal Institute of Technology (ETH), located in Zurich, which works more particularly on the conductor [26]. The iron yoke surrounding the solenoid is divided into three parts: (1) a barrel yoke, weighing 6,000 metric tons, and (2) two end-cap disks, weighing 2,000 metric tons each. The total weight of the CMS experiment is estimated at about 14,500 metric tons.

5 DIPOLE AND QUADRUPOLE MAGNETS

5.1 COORDINATE SYSTEM DEFINITIONS

Let $(\Omega, \vec{X}, \vec{Y}, \vec{Z})$ designate a rectangular coordinate system, and let us consider an accelerator ring whose design orbit is planar and is located in the $(\Omega, \vec{X}, \vec{Z})$, as represented in Figure 13. Furthermore, let O be a given point of the design orbit, and let $(O, \vec{x}, \vec{y}, \vec{z})$ designate a rectangular coordinate system associated with O, such that $\vec{y}$ and $\vec{Y}$ are one and the same and $\vec{z}$ is tangent to the design orbit at O. Throughout the paper, the *x*-axis defines the horizontal direction, the *y*-axis defines the vertical direction, and the *z*-axis corresponds to the main direction of particle motion.

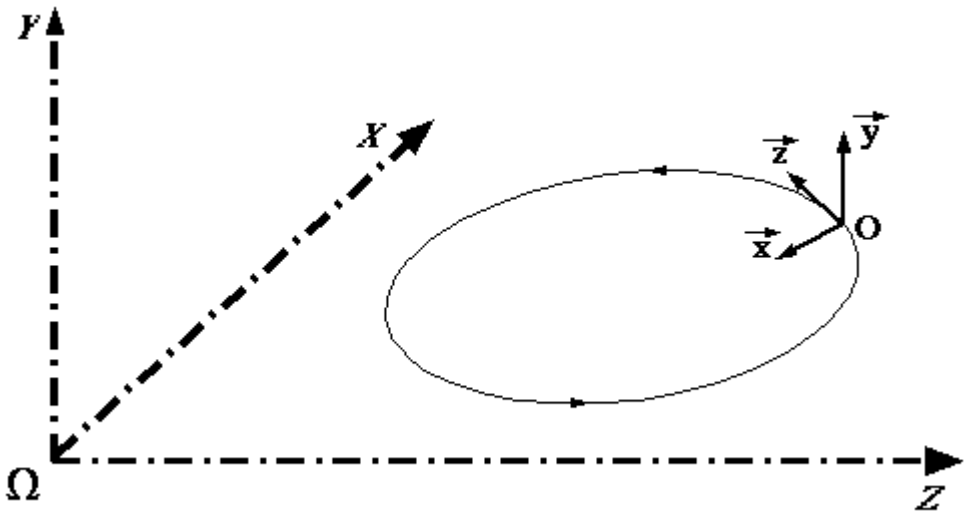

Figure 13. Coordinate systems associated with the design orbit of an accelerator ring.

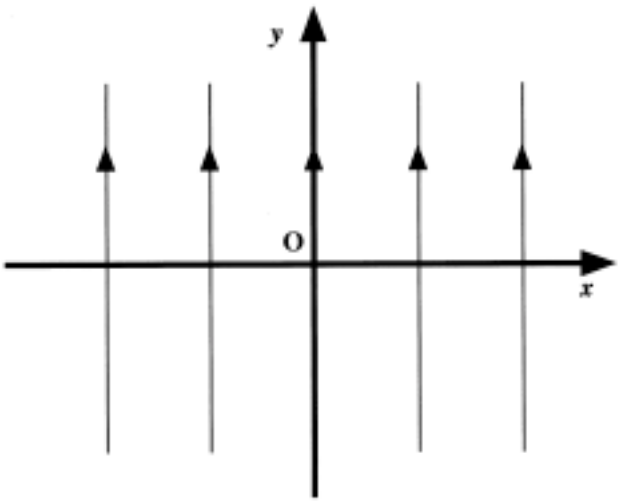

Figure 14. Ideal normal dipole magnet field lines.

5.2 NORMAL DIPOLE MAGNET

An ideal normal dipole magnet whose center is positioned at O is a magnet, which, within its aperture, produces an uniform magnetic flux density parallel to the *y*-axis and such that

$$B_x = 0 \qquad B_y = B_1 \qquad \text{and} \qquad B_z = 0 \tag{14}$$

where B_x, B_y and B_z are the *x*-, *y*- and *z*-components of the magnetic flux density, and B_1 is a constant referred to as the *dipole field strength* (in teslas). As represented in Figure 14, the field lines of an ideal normal dipole magnet are straight lines parallel to the *y*-axis.

A charged particle traveling along the direction of the *z*-axis through the aperture of a normal dipole magnet of length, l_{dip}, describes an arc of circle parallel to the horizontal $(\vec{x}, \vec{z})$ plane, and of radius of curvature, χ, determined by Eq. (3). The angular deflection, ϕ_{dip}, of the particle trajectory can be estimated as

$$\phi_{dip} \approx \frac{l_{dip}}{\chi} \tag{15}$$

Here, ϕ_{dip} is in radians, and l_{dip} and χ are in meters. The effect of a dipole magnet on a beam of charged particles can be compared to the effect of a prism on a light ray.

For the storage/collision phase of LHC at CERN, we have (see Table 1): l_{dip} = 14.2 m and χ = 2784.32 m. It follows from Eq. (15) that a single arc dipole magnet bends the proton trajectory by an angle $\phi_{dip} \approx 5.1$ mrad. Hence, a full (2π) rotation requires a total of 1232 arc dipole magnets.

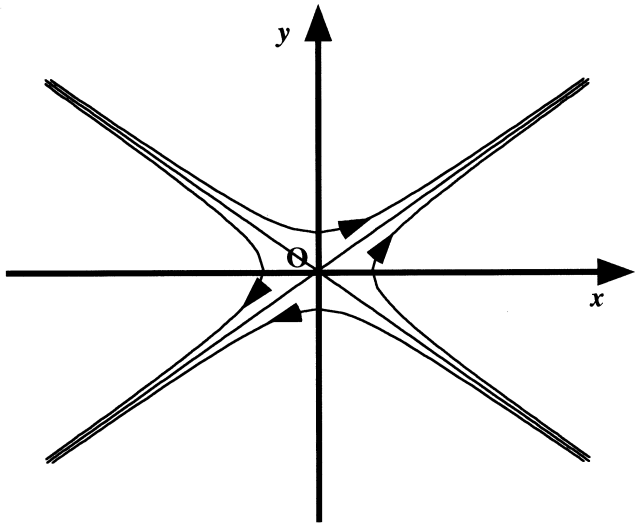

Figure 15. Ideal normal quadrupole magnet field lines.

5.3 NORMAL QUADRUPOLE MAGNET

An ideal normal quadrupole magnet whose center is positioned at O is a magnet, which, within its aperture, produces a two-dimensional magnetic flux density parallel to the $(\vec{x}, \vec{y})$ plane and such that

$$B_x = g\,y \qquad B_y = g\,x \qquad \text{and} \qquad B_z = 0 \tag{16}$$

where g is a constant referred to as the *quadrupole field gradient* (in teslas per meter). The field lines of an ideal normal quadrupole magnet are hyperbolae of center O whose asymptotes are the first and second bisectors (see Figure 15).

As illustrated in Figure 16(a) and Figure 16(b), a beam of positively charged particles traveling along the direction of the *z*-axis through the aperture of an ideal normal quadrupole magnet is horizontally focused and vertically defocused when g is positive. Conversely, the beam is vertically focused and horizontally defocused when g is negative. In reference to its action along the *x*-axis (on a beam of positively charged particles traveling in the positive *z*-direction), a magnet with a positive gradient is called a *focusing* quadrupole magnet, while a magnet with a negative gradient is called a *defocusing* quadrupole magnet.

To obtain a net focusing effect along both *x*- and *y*-axes, focusing and defocusing quadrupole magnets must be alternated in the magnet lattice [8].

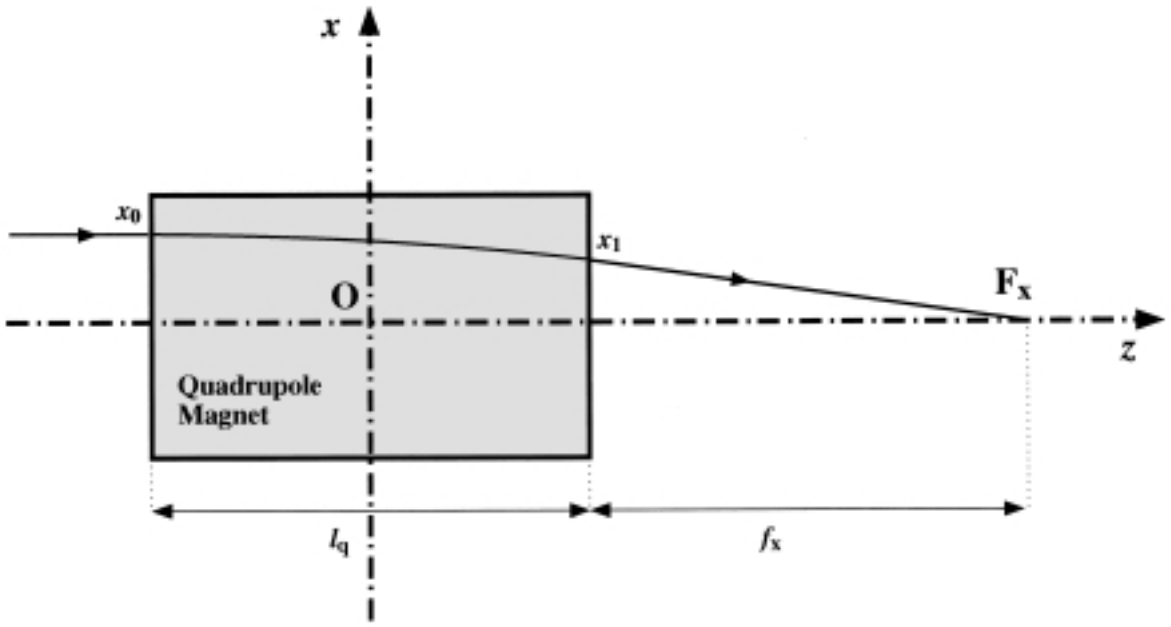

Figure 16(a). Horizontal focusing of positively charged particles circulating through the aperture of an ideal normal quadrupole magnet with a positive gradient.

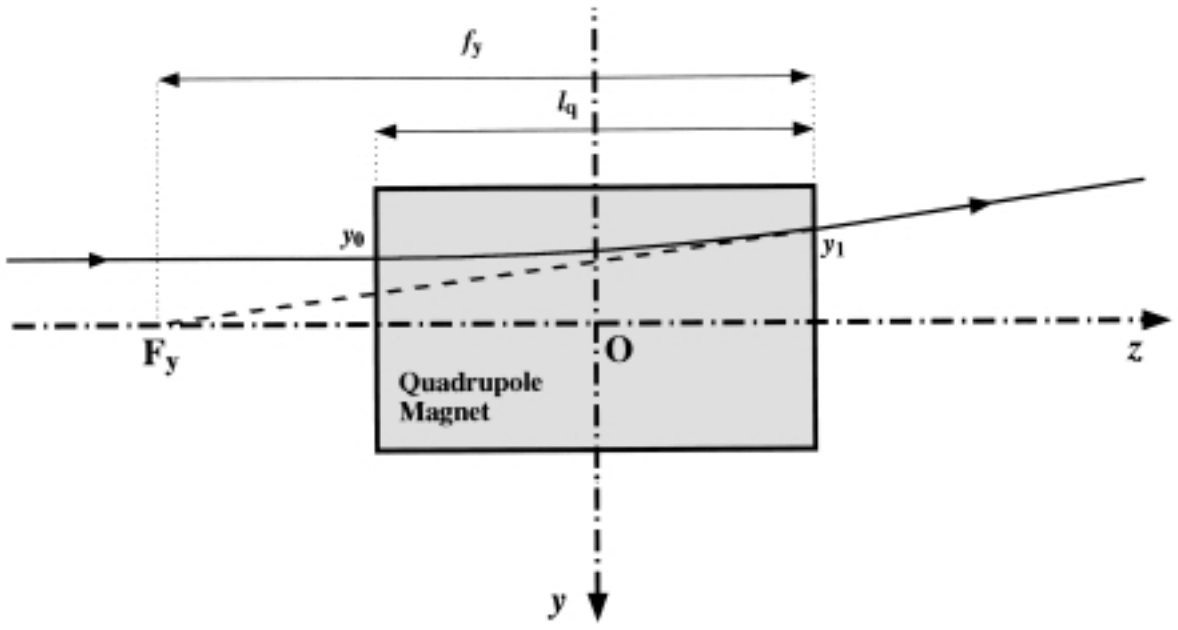

Figure 16(b). Vertical defocusing of positively charged particles circulating through the aperture of an ideal normal quadrupole magnet with a positive gradient.

The effects of focusing/defocusing quadrupole magnets on a beam of charged particles are similar to those of convex/concave lenses on a light ray. By analogy, and with the assumption that the transverse motions of the particles in the $(\vec{x}, \vec{y})$ plane are small compared to their longitudinal motion along the *z*-axis, the focusing effect of a normal quadrupole magnet of length, l_{quad}, can be characterized by the *focal length*, f_{quad}, given by

$$f_{\text{quad}} \approx \frac{1}{\sqrt{\kappa_{\text{g}}}} \cot\left(\sqrt{\kappa_{\text{g}}}\, l_{\text{quad}}\right) \tag{17}$$

while the defocusing effect, can be characterized by the focal length, f'_{quad}, given by

$$f'_{\text{quad}} \approx \frac{-1}{\sqrt{\kappa_{\text{g}}}} \coth\left(\sqrt{\kappa_{\text{g}}}\, l_{\text{quad}}\right) \tag{18}$$

In Eqs. (17) and (18), f_{quad} and f'_{quad} are taken from the magnet end where the beam exits [see Figure 16(a) and Figure 16(b)], and κ_{g} is the *normalized gradient*, which appears when solving the equations of motion

$$\kappa_{\text{g}} = \frac{q\, g}{m_{\text{q}}\, \gamma_{\text{q}}\, v_{\text{q}}} \tag{19}$$

Here, q is the particle charge, m_{q} is the particle mass at rest, v_{q} is its velocity and γ_{q} is the relativistic Lorentz factor defined by Eq. (4).

Assuming again that the particle total energy, $\mathcal{E}_{\text{q}} = m_{\text{q}}\, \gamma_{\text{q}}\, \text{c}^2$, is far greater than its energy at rest, $\mathcal{E}_{\text{q,0}} = m_{\text{q}}\, \text{c}^2$ (where c is the speed of light), Eq. (19) can be recast in the form

$$\kappa_{\text{g}} \approx \frac{\text{c}\, q\, g}{\mathcal{E}_{\text{q}}} \approx \frac{0.3\, q_{\text{e}}\, g}{\mathcal{E}_{\text{GeV}}} \tag{20}$$

Here, κ_{g} is in $(\text{rad/m})^2$, q_{e} is in units of electron charge, g is in T/m, and $\mathcal{E}_{\text{GeV}}$ is in GeV.

Equations (17) and (18) show that in order to keep the focal lengths constant during the acceleration phase, κ_{g} must be kept constant, and Eq. (20) shows that in order to keep κ_{g} constant, g must be raised in proportion to beam energy. As a result, during the acceleration phase, the arc dipole and quadrupole magnets are ramped up together so as to ensure that the bending dipole field strength and the focusing/defocusing quadrupole field gradients track the beam energy. As already discussed, this is one is of the operating principles of a synchrotron.

For the storage/collision phase of the LHC at CERN, we have (see Table 1): g = 223 T/m, l_{quad} = 3.1 m, and $\mathcal{E}_{GeV} \approx 7000$ GeV. It follows from Eq. (20) that: $\kappa_g \approx 0.01$ (rad/m)^2, while Eq. (17) yields: $f_{quad} \approx 32.7$ m, and Eq. (18) yields: $f_{quad} \approx -34.8$ m. The LHC arcs count a total number of 392 quadrupole magnets.

6 DETECTOR MAGNET CONFIGURATIONS

6.1 ON THE USE OF DETECTOR MAGNETS

Particle physics experiments are made up of various kinds of detectors, which measure the energy and determine the trajectories of interaction products. In addition, they usually include a large magnet system, embedded in the detector array, which produces a strong magnetic flux density (a few teslas) in a large volume (up to tens of cubic meters) around the interaction points. This magnetic flux density causes a bending of the charged particles' trajectories, with radii of curvature which are directly proportional to the particles' charge and energy. The detection of such bending and the determination of its parameters can provide additional informations on the nature of interaction products and on their kinematics.

6.2 SOLENOIDAL CONFIGURATION

The simplest magnetic configuration used in particle detectors is that of a solenoid. As an illustration, Figure 17 shows an artist view of the superconducting solenoid for the CMS experiment at CERN (see section 4.6.4).

An ideal solenoid, positioned around O and of z-axis, is a magnet, which, within its aperture, produces an uniform magnetic flux density, parallel to the z-axis and such that

$$B_x = 0 \qquad B_y = 0 \qquad \text{and} \qquad B_z = B_0 \tag{21}$$

where B_0 is a constant, referred to as the axial field strength (T).

The main advantage of a solenoid is the straightforwardness of its design and of its fabrication, but it has two main disadvantages: (1) it requires a large and heavy iron yoke, and (2) it is not very efficient for particles whose momenta are at small angles with respect to the z-axis. The iron yoke is used to return the magnetic flux lines and is usually integrated in the calorimeters' designs. For example, in the case of CMS, the iron yoke (depicted in Figure 12) is part of the muon calorimeters. The inefficiency of a solenoidal configuration for small-angle particles stems from the fact that, in Lorentz law [see Eq. (2)], only the component of the magnetic flux density that is perpendicular to the particle velocity can act on its motion. As a result, particles moving almost parallely to the z-axis are little affected by the solenoidal magnetic flux density, and, therefore, are more difficult to analyze.

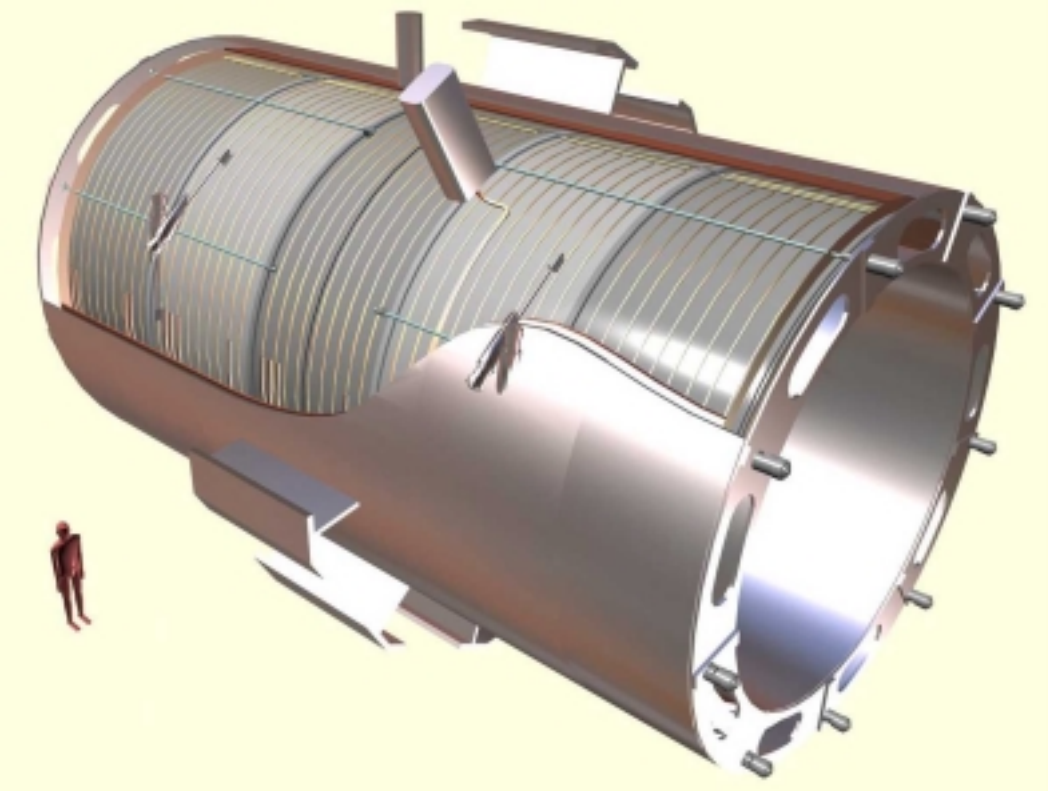

Figure 17. Solenoid for the CMS experiment at CERN.

6.3 TOROIDAL CONFIGURATION

An alternate configuration for a detector magnet is that of a toroid.

Let $(O, \vec{u}_r, \vec{u}_\theta, \vec{z})$ designate a cylindrical coordinate system, deduced from the rectangular coordinate system $(O, \vec{x}, \vec{y}, \vec{z})$ by a rotation around the *z*-axis. An ideal toroid positioned around O and whose main axis is the *z*-axis, is a magnet, which, within an axi-symmetric volume around the *z*-axis, produces an uniform magnetic flux density that is purely circumferential

$$B_r = 0 \qquad B_\theta = B_0 \qquad \text{and} \qquad B_z = 0 \tag{22}$$

where B_r and B_θ are the radial and azimuthal components of the magnetic flux density and B_0 is a constant.

Such magnetic configuration offers at least two advantages: (1) the magnetic flux lines are confined and no iron yoke is needed, and (2) the magnetic flux density is almost always perpendicular to the interaction products' trajectories, providing a maximum bending efficiency. The main disadvantage of a toroid is that it is a far more complicated structure than a solenoid and that it requires a sophisticated mechanical design and detailed analyses of failure modes.

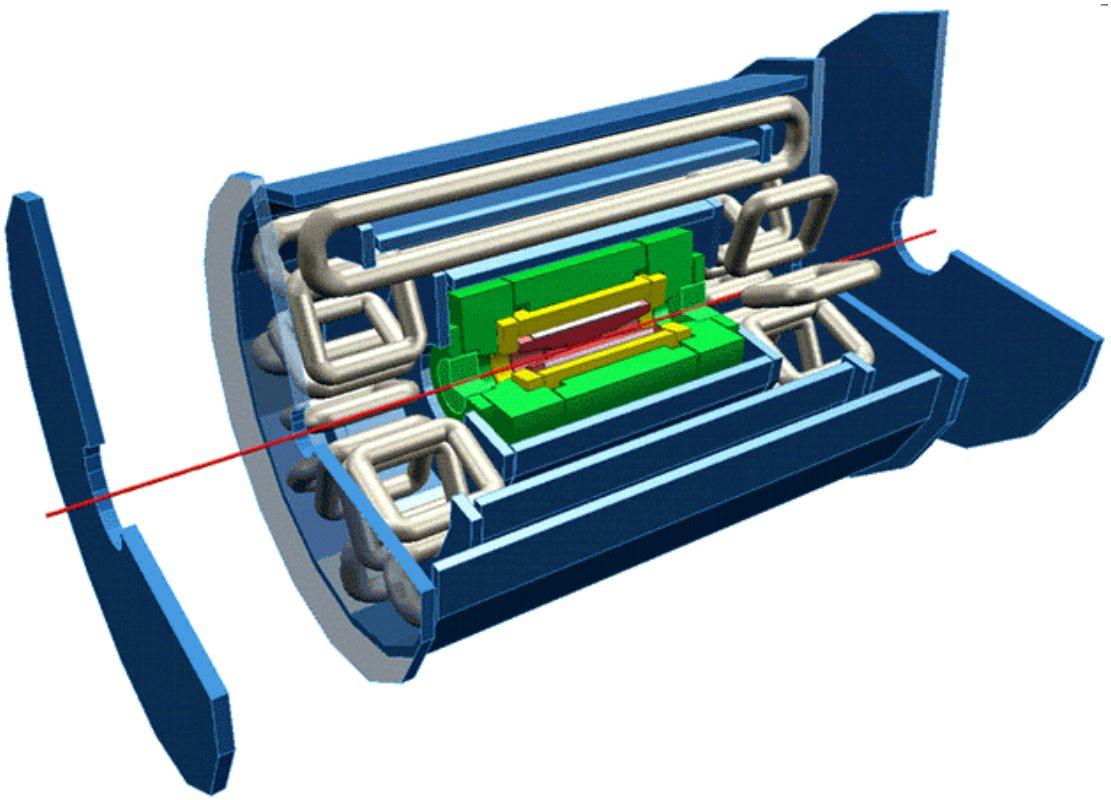

Figure 18. Approximation of toroidal configurations by racetrack-type coils in the ATLAS experiment at CERN.

In practice, the toroidal configuration is approximated by a set of identical, planar coils mounted axi-symmetrically around the *z*-axis. As an illustration, the Barrel Toroid (BT) of the ATLAS experiment at CERN (see section 4.6.4 and Figure 18) is made up of eight, superconducting, 25-m-long, 5-m-wide racetrack coils, positioned at a radius of about 5 m around the *z*-axis, and producing an average circumferential field of the order of 1.2 T. In addition, the ATLAS magnet system includes two smaller toroids located in the end caps (also shown in Figure 18), made up again of eight, superconducting 4.3-m-long, 3.8-m-wide racetrack-type coils, and producing an average circumferential field of the order of 2.5 T. It is completed by a 5.3-m-long superconducting solenoid, with a diameter of about 2.5 m, positioned at the center of the experiment, and producing an axial field of 2 T. The solenoid is surrounded by an iron yoke and it is magnetically independent from the toroids. ATLAS will be one of the largest and most complex particle physics experiments ever built.

ACKNOWLEDGMENTS

The author wishes to thank C. Wyss for his continuous interest and support and F. Kircher and R. Ostojic for insightful comments on the manuscript.

REFERENCES

[1] C. Quigg, *The Third Bernard Gregory Lectures*, CERN/89–11, Geneva: CERN, December 1989.

[2] E.O. Lawrence and M.S. Livingston, "A method for producing high speed hydrogen ions without the use of high voltages," *Phys. Rev.*, Vol. 37, p. 1707, 1931.

[3] E.O. Lawrence and M.S. Livingston, "The production of high speed light ions without the use of high voltages," *Phys. Rev.*, Vol. 40, pp. 19–35, 1932.

[4] T. Stammbach, "Introduction to cyclotrons." In S. Turner (ed.), *Proc. of CERN Accelerator School on Cyclotrons, Linacs and their Applications*, CERN 96–02, Geneva: CERN, pp. 113–138, March 1996.

[5] *LEP Design Report, Vol. 2: The LEP Main Ring*, CERN–LEP/84–01, Geneva: CERN, June 1984.

[6] J.M. Baze, H. Desportes, R. Duthil, J.M. Garin, Y. Pabot, J. Heitzmann, M. Jacquemet, J.P. Jacquemin, F. Kircher, J.C. Languillat, J. Le Bars, A. Le Coroller, C. Lesmond, J.C. Lottin, J.P. Lottin, C. Mathis, C. Meuris, J.C. Sellier and C. Walter, "Design, construction and test of the large superconducting solenoid ALEPH," *IEEE Trans. Magn.*, Vol. 24 No. 2, pp. 1260–1263, 1988.

[7] P. Lefèvre and T. Petterson (eds.), *The Large Hadron Collider: Conceptual Design*, CERN/AC/95–05(LHC), Geneva: CERN, 20 October 1995.

[8] S. Humphries, Jr., *Principles of Charged Particle Acceleration*, New York: John Wiley & Sons, 1986.

[9] D.A. Edwards and M.J. Syphers, *An Introduction to the Physics of High Energy Particle Accelerators*, New York: John Wiley & Sons, 1993.

[10] H. Padamsee, J. Knobloch and T. Hays, *RF Superconductivity for Accelerators*, New York: John Wiley & Sons, 1998.

[11] C. Wyss (ed.), *LEP Design Report, Vol. 3: LEP2*, CERN–AC/96–01, Geneva: CERN, June 1996.

[12] M. Peckeler, "Experience with superconducting cavity operation in the TESLA Test Facility," *Proc. of 1999 Particle Accelerator Conference (PAC 1999)*, IEEE Catalogue 99CH36366, pp. 245–249, 1999.

[13] R. Brinkmann, "Status of the design for the TESLA linear collider," *Proc. of 1995 Particle Accelerator Conference (PAC 1995)*, IEEE Catalogue 95CH35843, pp. 674–676, 1996.

[14] G. Arduini, R. Assman, R. Bailey, A. Butterworth, P. Collier, K. Cornelis, M. Lamont, G. Morpurgo, P. Raimondi, G. Roy, J. Wenninger, "LEP operation and performance with 100 GeV colliding beams," *Proc. of 7th European Particle Accelerator Conference (EPAC 2000)*, pp. 265–267, 2000.

[15] K.-H. Mess, P. Schmüser and S. Wolf, *Superconducting Accelerator Magnets*, Singapore: World Scientific, 1996.

[16] K. Tsuchiya, T. Ogitsu, N. Ohuchi, T. Ozaki, N. Toge and H. Sakurabata, "Superconducting magnets for the interaction region of KEKB," *IEEE Trans. Appl. Supercond.*, Vol. 9 No. 2, pp. 1045–1048, 1999.

[17] J.T. Seeman, "Commisionning results of the KEKB and PEP-II B-Factories," *Proc. of 1999 Particle Accelerator Conference (PAC 1999)*, IEEE Catalogue 99CH36366, pp. 1–5, 1999.

[18] H. Desportes, "Advanced features of very large superconducting magnets for SSC and LHC detectors," *IEEE Trans. Mag.*, Vol. 30 No. 4, pp. 1525–1532, 1994.

[19] R. Ostojic, T.M. Taylor and S. Weisz, "Systems layout of the low-β insertions for the LHC experiments," *Proc. of 1997 Particle Accelerator Conference (PAC 1997)*, IEEE Catalogue 97CH36167, pp. 3696–3698, 1998.

[20] H.H.J. ten Kate, "The superconducting magnet system for the ATLAS detector," *IEEE Trans. Appl. Supercond.*, Vol. 9 No. 2, pp. 841–846, 1999.

[21] A. Yamamoto, T. Kondo, Y. Doi, Y. Makida, K. Tanaka, T. Haruyama, H. Yamaoka, H. ten Kate, L. Bjorset, K. Wada, S. Meguro, J.S.H. Ross, and K.D. Smith, "Design and development of the ATLAS Central Solenoid," *IEEE Trans. Appl. Supercond.*, Vol. 9 No. 2, pp. 852–855, 1999.

[22] J.M. Baze, C. Berriaud, C. Curé, A. Daël, H. Desportes, R. Duthil, B. Gallet, F.P. Juster, C. Lesmond, C. Mayri, and Y. Pabot, "Progress in the design of a superconducting toroidal magnet for the ATLAS detector on LHC," *IEEE Trans. Mag.*, Vol. 32 No. 4, pp. 2047–2050, 1996.

[23] A. Daël, J. Belorgey, C. Berriaud, R. Berthier, D. Cacaut, H. Desportes, B. Gallet, B. Gastineau, M. Jacquemet, F.P. Juster, C. Lesmond, C. Mayri, Y. Pabot, J.M. Rey, H. van Hille, Z. Sun, E. Acerbi, F. Alessandria, G. Ambrosio, F. Broggi, L. Rossi, M. Sorbi, G. Volpini, "Progress in the design of the barrel toroid magnet for the ATLAS experiment and associated R&D at CEA-Saclay and INFN-Milano," *Proc. of 15th International Conference on Magnet Technology (MT 15)*, Beijing: Science Press, pp. 92–95, 1998.

[24] D.E. Baynham, J. Butterworth, F.S. Carr, M.J.D. Couthold, D.A. Cragg, C.J. Densham, D. Evans, E. Holtom, S.J. Robertson, D. Sole, and E.F. Towndrow, "Engineering design and optimization of the superconducting End Cap Toroid magnets for the ATLAS experiment at LHC," *IEEE Trans. Appl. Supercond.*, Vol. 9 No. 2, pp. 856–859, 1999.

[25] J.C. Lottin, H. Desportes, C. Lesmond, C. Lyraud, C. Pes, and A. Hervé, "Conceptual design of the CMS 4 Tesla solenoid," *Adv. Cryo. Eng.*, Vol. 41A, pp. 819–825, 1996.

[26] F. Kircher, B. Levesy, Y. Pabot, D. Campi, B. Curé, A. Hervé, I.L. Horvath, P. Fabbricatore, and R. Musenich, "Status report on the CMS superconducting solenoid for LHC," *IEEE Trans. Appl. Supercond.*, Vol. 9 No. 2, pp. 837–840, 1999.